Lindgren, Mari; Huttunen-Saarivirta, Elina; Peltola, Heljä; Romu, Jyrki; Sarikka, Teemu; Hänninen, Hannu; Pohjanne, Pekka

Crevice corrosion of stainless steels 904L, 2205 and 2507 in high-temperature sulfuric acid solution containing chlorides: Influence of metal cations

Published in:
Corrosion

DOI:
10.5006/2565

Published: 01/02/2018

Document Version
Peer-reviewed accepted author manuscript, also known as Final accepted manuscript or Post-print

Please cite the original version:
Lindgren, M., Huttunen-Saarivirta, E., Peltola, H., Romu, J., Sarikka, T., Hänninen, H., & Pohjanne, P. (2018). Crevice corrosion of stainless steels 904L, 2205 and 2507 in high-temperature sulfuric acid solution containing chlorides: Influence of metal cations. *Corrosion*, *74*(2), 225-240. https://doi.org/10.5006/2565

Crevice corrosion of stainless steels 904L, 2205 and 2507 in high-temperature sulfuric acid solution containing chlorides: Influence of metal cations

M. Lindgren[1,*], E. Huttunen-Saarivirta[2], H. Peltola[1], J. Romu[3], T. Sarikka[3], H. Hänninen[3], P. Pohjanne[2]

[1] Outotec (Finland), Pori Research Center, Kuparitie 10, 28101 Pori, Finland

[2] VTT Technical Research Centre of Finland Ltd, Kemistintie 3, 02044 Espoo, Finland

[3] Aalto University School of Engineering, P.O. Box 14100, FI-02150 Espoo, Finland

* Corresponding author. Contact by e-mail: mari.lindgren@outotec.com or by phone: +358408297293

Abstract

Crevice corrosion influences the integrity of materials in many industrial sectors, such as hydrometallurgy. The conditions in hydrometallurgical processes are severe, with high concentrations of sulfuric acid leachant as well as high chloride impurity, oxygen and metal cation contents. In this study, crevice corrosion behaviour of highly-alloyed austenitic and duplex stainless steels is investigated in aerated high-temperature sulfuric acid solution with 1 g/l chlorides in the presence of three types of metal cations: Fe^{3+}, Cu^{2+}, and Fe^{2+}. The experimental work contained determination of the oxidizing capacity of the solutions, immersion crevice corrosion tests followed by characterization of the corrosion attack, and potentiodynamic polarization measurements. The results showed that the alloy with the highest PREN-value, 2507, was not susceptible to crevice corrosion under the test conditions. In the case of alloys 904L and 2205 of relatively equal PREN-values, the extent and nature of crevice corrosion attack was different and dependent on the ratio

of activities of chlorides to sulfates and the type of metal cations. The results are presented and discussed in the light of IR drop mechanism.

Keywords: Crevice corrosion; stainless steel; sulfuric acid; cations; chloride.

1. Introduction

Hydrometallurgical treatment of ores has been promoted by declining ore grades and the emergence of secondary raw material sources. E.g., copper ores that are too low-grade for concentration process or contain such undesirable impurities that they cannot be smelted may be refined by hydrometallurgical route [1]. In the hydrometallurgical treatment of mineral raw materials, sulfuric acid is a common leaching agent due to its low cost, environmental friendliness and possibility for regeneration. The use of elevated temperatures significantly accelerates the leaching kinetics and therefore typical process temperatures approach the boiling point of the solution, being about 100ºC. From the corrosion point of view, chlorides are the main impurities in the leaching process and they may originate either from raw materials or from make-up water. Typical chloride concentrations are in the magnitude of a few hundreds of milligrams per liter. Oxygen and ferric ions, Fe^{3+}, the latter also originating from the mineral raw materials, can act as oxidants to enhance the leaching. Because of this, the redox potential of the solution is high, promoting localized, i.e., pitting and crevice, corrosion of passivating metals if critical values are exceeded. Ferrous iron, Fe^{2+}, is always present and has an inhibiting effect on uniform corrosion of the main construction materials in sulfuric acid environment [2]. Cupric ions, Cu^{2+}, if present, are beneficial for the uniform corrosion resistance of passivating alloys but may promote localized corrosion.

The aggressive nature of the leaching environment is reflected to the materials selection. Depending on the exact solution chemistry, austenitic corrosion-resistant alloys, such as 904L, and duplex ferritic-austenitic corrosion-resistant stainless steels, such as 2205 or 2507, can be selected. However, crevice corrosion is the most difficult corrosion mode to take into account in the

choice of materials, as crevices may vary from the geometrical and structural features, such as crevices created by bolts, nuts, welds and flange connections, to those created by an unpredictable formation of adherent deposits or accumulation of solids from the process.

The current understanding of crevice corrosion of passivating metals is based on three models [3]: (1) passive dissolution leading to a gradual acidification and a general passivity breakdown [4], (2) so-called IR (ohmic) drop mechanism [5], and (3) stabilization of metastable pits by an occluded crevice geometry [6, 7], or a combination of these. Typically, the generation of the more aggressive environment in the pit or crevice involves acidification of the environment and the ingress of negative chloride ions to counterbalance the positively charged metal cations, and the crevice environment depletes with respect to oxygen. The special characteristics of the hydrometallurgical leaching solutions are that the leaching solutions are very acidic to start with (pH<1) and the solutions contain negatively charged sulfate ions in addition to chlorides and oxidizers, probably also influencing the crevice corrosion behavior.

In general, the IR drop mechanism is widely acknowledged to explain the crevice corrosion of passive metals with the changes in the solution composition inside the crevice aggravating the chemical environment. According to the IR drop mechanism, the localized corrosion starts when:

$IR > \Delta\emptyset^*$ (Equation 1)

where:

$\Delta\emptyset^* = E_{SURF} - E_{A/P}$ (Equation 2)

In these equations, I is the current flowing out of the crevice, R is the resistance of the crevice electrolyte, and $\Delta\emptyset^*$ is the difference between the applied potential E_{SURF} and the electrode potential of the active/passive transition $E_{A/P}$. In some cases [8], e.g., Ni in sulfuric acid [9], the

active peak originally exists in the polarization curve and immediate crevice corrosion ensues. In contrast, in less corrosive environments [10] or for more corrosion-resistant alloys [11,12], an incubation period is required for the active peak to appear. This can occur when i) the passive current increases [13] or metastable pitting gives raise to current (I increases), ii) the potential range of the active peak increases ($E_{A/P}$ increases) due to an increase in temperature or a change in the electrolyte composition (pH [14], chlorides), iii) R increases due to the formation of constriction by gas bubbles or corrosion products [15], or iv) the corrosion potential of applied potential E_{SURF} shifts in the negative direction. Then the crevice corrosion initiates at some distance $x_{A/P}$ from the crevice mouth.

Considering only the $IR>\Delta\emptyset^*$ criterion, crevice corrosion is less likely when oxidants with noble electrode potential are used, as $\Delta\emptyset^*$ increases. This has been demonstrated to hold true for iron in strongly buffered solutions or in solutions close to the hydrolysis equilibrium, i.e., in cases where the pH change is precluded [16]. Abdulsalam and Pickering investigated the effect of the oxidizing power on the electrode potential profile and in-situ measured crevice corrosion for nickel in 1N H_2SO_4 under conditions of effective convective mixing of the crevice and bulk electrolytes [9]. In other words, in their experimental system the composition of the crevice electrolyte did not change and hence pure IR drop effect was measured. They stated that both higher E_{SURF} and increase in the amount of oxidant (oxygen) available in the crevice meant the lower susceptibility or rate of crevice corrosion. Abdulsalam et al. [17] further demonstrated by applying an external potential that the higher the applied potential the lower the crevice corrosion rate. In contrast, a different view emerges from the studies in which the composition of the crevice electrolyte is allowed to change with time. Sridhar and Dunn increased the applied potential in steps and monitored potential, current density, Cl^- concentration and pH of the bulk in the mouth and tip of the crevice [11]. They observed that the environment inside the crevice was altered only when the external potential was maintained above a certain value. When this critical value was exceeded, there was an incubation period followed by a rapid increase in the current density. This event was succeeded

by a decrease in pH and potential in the crevice. Similarly, in potentiostatic and open-circuit tests of Alloy 825 in 1,000 ppm Cl^- at 95ºC, higher applied potentials were conducive to faster crevice corrosion initiation times [18]. This means that, in contrast to pure IR experiments, when the environment was allowed to change, the higher applied potentials promoted the occurrence of crevice corrosion. This is consistent with the establishment of various critical potentials for the prediction of the occurrence of crevice corrosion in stainless steels and nickel-based alloys [19,20].

Crevice corrosion resistance of austenitic and duplex stainless steels can be influenced by alloying [21,22]. In duplex stainless steels, the two-phase microstructure implies that the austenite and ferrite phases may be attacked differently based on their different chemical composition and thus polarization behavior within the crevice [23]. In the zone of the most severe attack, the microstructural features are often no longer distinguishable, but in the areas of lighter attack, either ferrite [22-24] or austenite [25] may be preferentially attacked even within different locations of a single sample.

In this study, crevice corrosion behavior of highly-alloyed austenitic and duplex stainless steels is investigated in high-temperature sulfuric acid solution with 1 g/l chlorides, under the conditions simulating leaching processes of ores. The focus is on the effect of the amount and nature of metal cations on the degradation of the materials. Instead of using an external current source to apply the potential to the sample, oxidizing ions Fe^{3+} and Cu^{2+}, and metal cations Fe^{2+} are employed to see whether their chemical nature has an influence besides their different electrode potentials. The extent and characteristics of attack as well as reasons for dissimilar behavior of the three stainless steel grades are described and discussed in this paper.

2. Experimental

2.1. Materials

Studies were conducted for three stainless steel grades: AISI 904L (EN 1.4539, UNS N08904), 2205 (EN 1.4462, UNS S32205) and 2507 (EN 1.4410, UNS S32750). The typical chemical compositions of the alloys and their pitting resistance equivalent numbers, PREN = Cr + 3.3Mo + 16N, are shown in Table 1. The surface finish of the test materials was 2E, i.e., annealed, shot blast and pickled. The materials were obtained as sheets with the thickness of 3 mm, of which the specimens of the size of 50 mm x 50 mm were laser cut. The edges of the specimens were ground and treated with a pickling paste (Polinox P Rapid) for 60 min in order to remove the chromium-depleted surface layer possibly induced by laser cutting, and so to repassivate the edges. Before the tests, the specimens were cleaned with ethanol, rinsed with deionized water, and dried.

2.2. Methods

2.2.1. Immersion crevice corrosion tests

Prior to the attachment of the crevice formers, the specimens were weighed. The specimens were then equipped with flat or serrated polytetrafluoroethylene (PTFE) crevice formers of the inner and outer diameters of 12.5 mm and 27.6 mm, respectively, which were tightened onto the surfaces to a torque of 6 Nm using a moment wrench. The serrated crevice formers contained 1mm wide and 1 mm thick grooves. The stainless steel specimens together with the crevice formers were attached to an annular specimen holder made of titanium, and the ring was placed on the bottom of the reactor. The specimens were insulated from the titanium bolts by PTFE. The reactors used in the experiments were heated and thermally insulated glass reactors of the liquid volume of 5 l.

Four experiments with equal sulfuric acid, 50 g/l (0.5 M) and chloride concentrations, 1 g/l (0.028 M), but with different additions of oxidizing ions were carried out. In the experiments, three types of cations: ferric iron, Fe^{3+}, cupric ion, Cu^{2+} and ferrous iron, Fe^{2+}, at the initial concentration of 5 g/l were included, one type of cation in each test. Additionally, the influence of the ion concentration, 0.5 g/l vs. 5 g/l, of ferric iron, Fe^{3+}, was examined in the fourth experiment. In all cases, the solution temperature was 90ºC and the immersion time of the samples was four weeks (672 h). The target parameters of the test solutions are given in Table 2. Only one specimen of each material was tested using the flat crevice formers, but parallel tests were run with serrated crevice formers allowing the detected trends to be verified.

The test solutions were prepared from reagent grade chemicals and deionized water. The addition of chlorides was made in the form of hydrochloric acid, and the additions of cations as sulfates: $Fe_2(SO_4)_3$, $CuSO_4$ and $FeSO_4$. The solutions were analyzed before and after the tests in order to check the match with the target values and to reveal the changes during the tests. The redox potentials and the pH-values were measured from the initial test solutions at room temperature and after the solutions had reached the test temperature (90°C), and from the final solutions at the end of the tests. In the initial test solutions, the open circuit potentials (OCP) of 904L stainless steel were additionally measured at 90°C. In both measurements, redox and OCP, an Ag/AgCl (saturated KCl) reference electrode was used. The solutions were stirred by rotary magnets (8 mm x 40 mm) throughout the tests. Minor vaporization occurred from the solutions during the four-week test period, although the reactors were sealed with lids. This was compensated by deionized water additions on regular basis.

2.2.2. Characterization

After the tests, the specimens were photographed (Nikon D 700), and inspected both visually and under a stereo microscope (Zeiss Stemi 2000-C) in order to evaluate the occurrence of corrosion.

Based on the stereomicroscopy inspections, the most interesting specimens were selected for scanning electron microscopy (SEM) examinations. SEM studies were conducted for the specimens in plane and cross-section using a Zeiss Merlin VP Compact SEM equipped with a Bruker X-flash energy dispersive spectrometer (EDS) and a Bruker Quantax electron backscattered diffractometer (EBSD).

2.2.3. Electrochemical measurements

The three stainless steel grades were subjected to potentiodynamic polarisation measurements to reveal their overall corrosion behaviour in the test solutions and in simulated crevice solutions. In order to have the specimens in an identical condition, the surfaces were ground to 600 grit surface finish. The measurements were carried out using an Avesta cell, each of the stainless steel grades as the working electrode, platinum as the counter electrode and an Ag/AgCl (saturated KCl) or a saturated calomel electrode (SCE) as reference electrodes. For the uniform presentation of the results, all potential values in this paper are presented with respect to Ag/AgCl (saturated KCl).The measurements were carried out from -50 mV vs. OCP to 960 mV vs. ref and back. The scan rate in the measurements was 0.167 mV/s.

The anodic polarisation measurements for all three stainless steels were performed in the electrolyte that was the base in all four test solutions in immersion crevice corrosion experiments, i.e., aqueous solution heated to 90°C and containing 50 g/l sulfuric acid, H_2SO_4, and 1 g/l chlorides, Cl^- (added as HCl). Similarly, measurements for all three grades were conducted in concentrated chloride solutions containing fivefold amount of chlorides compared to the base solution, i.e., 50 g/l sulfuric acid and 5 g/l chlorides (added as HCl). Additionally, for 904L, the influence of the oxidizing ions (adding 0.5 and 10 g/l of Fe^{3+} in the base solution), chloride concentration (adding 0, 1, 5 and 10 g/l of Cl^- in the base solution), and the addition of sulfate, SO_4^{2-} (45 g/l as Na_2SO_4 into the solution containing 50 g/l H_2SO_4 and 5 g/l Cl^-) were investigated.

3. Results

3.1. Solutions and their oxidation capacity

The analyses of the solutions before the immersion crevice corrosion tests are presented in Table 3. The table shows that the measured initial compositions were consistent with the targeted ones. In Solutions 1 and 4 (5 g/l and 0.5 g/l Fe^{3+}), the dissolved iron was almost totally in ferric form, as intended. In turn, in Solution 3 (5 g/l Fe^{2+}), a minor part of the dissolved iron was in ferric (Fe^{3+}) form, although the addition was made as ferrous sulfate (Fe^{2+}). This occurred consistently when the solution preparation procedure was repeated. The valence of copper ions in Solution 2 was not analyzed, but the addition was made as Cu^{2+} ions.

The equilibrium concentrations, activities and pH of the solutions as a function of temperature were calculated with the HSC Software [26] both for the target compositions (Table 2) and the measured compositions (Table 3). The calculations took into account the non-ideality of the solution by using the Pitzer's model to describe ion-ion interactions. Table 4 summarizes the calculated activities for chlorides and sulfates, their ratios and calculated pH values for solutions at 23°C and 90°C. Despite a relatively high sulfuric acid concentration, not much sulfate ions, SO_4^{2-}, existed in the equilibrium solutions and their activities were low. This is because sulfuric acid does not dissociate completely in aqueous media to H^+ and SO_4^{2-} ions and an intermediate species, bisulfate, HSO_4^-, is formed. At moderate temperatures and concentrations, bisulfate ion does not completely dissociate further to H^+ and SO_4^{2-} ions, so H^+ and HSO_4^- remain as the major species in the solution [27]. The calculated ratio of the activities of chlorides and sulfates varied between the solutions. The highest and the lowest chloride activity to sulfate activity ratios, 15.5 and 7.2, were determined for the solutions with 0.5 g/l and 5 g/l ferric iron, respectively. The corresponding ratios for the copper and ferrous iron containing solutions were intermediate to those and had relatively equal values, 9.8 and 9.2. The calculated pH-values showed similar trends with temperature as the experimental

ones. However, the lack of a clear correlation between the calculated and the measured pH-values in different solutions reflects the fact that at this high sulfuric acid concentration, pH is not a sensitive measure of the solution acidity any more.

As shown in Table 3, the redox potential, i.e., the oxidation capacity of the solution, was the highest for the solutions with ferric iron: Solution 1 (Fe^{3+} = 5 g/l) had the redox potentials of 510 and 680 mV at 23°C and 90°C respectively, and Solution 4 (Fe^{3+} = 0.5 g/l) had the redox potential values of 410 and 680 mV. This is in line with the results of Yue et al. [28] who stated that the redox potential of a Fe^{3+}/Fe^{2+} couple in the sulfuric acid solution is a function of the ratio of ferric to ferrous iron and the absolute amounts have only a minor influence. These solutions were followed in the oxidation capacity by Solution 3 (Fe^{2+} = 5 g/l; 340 and 440 mV). The oxidation capacity was lowest for Solution 2 at 23°C (Cu^{2+} = 5 g/l, 290 and 440 mV), but the value at 90ºC was at the same level as in the Fe^{2+}-containing solution. The redox potential values systematically increased by 33-65% during heating depending on the solution composition. To sum up Tables 3 and 4, at the test temperature of 90°C, the redox potentials were identical for the solutions containing ferric iron (Solutions 1 and 4), but they differed with respect to the ratio of the activities of chlorides and sulfates, 7.2 and 15.5 for the ferric iron concentrations of 5 g/l and 0.5 g/l, respectively. In the case of the test solutions containing copper (Solution 2) and ferrous iron (Solution 3), both the redox potential and the ratio of the activities of chlorides and sulfates were equal.

Composition of the test solutions after the tests is given in Table 5. Comparison of the final and the initial solution compositions enables few observations to be made. In the solutions containing Fe^{3+}, Solution 1 (5 g/l) and Solution 4 (0.5 g/l), some of the initial Fe^{3+} transformed into Fe^{2+}, with the redox potential also being lowered as compared to the initial value. The total Fe content was also higher than initially, evidently due to the corrosion of the specimens. In Solution 3 (5 g/l Fe^{2+}), some of the original Fe^{2+} transformed into Fe^{3+} accompanied by a rise in the oxidation capacity. In

Solutions 1 (5 g/l Fe^{3+}) and 2 (5 g/l Cu^{2+}), a slight increase in all measured concentrations was observed. As the contents of all constituents were higher than initially this indicates a slight evaporation of water during the experiment. The increase in the total dissolved iron content in Solution 2 was due to the corrosion of the specimens, similarly to the detected Cu^{2+} in Solution 1.

The OCP records of the 904L electrode, measured for two hours from the onset of the experiments in each test solution in the beginning of the experiment, are presented in Figure 1. The highest values were obtained in Solutions 1 (5 g/l) and 4 (0.5 g/l) with ferric iron, consistent with the redox potential measurements. Distinct from the observation that the redox potential does not depend on the amount of ferric iron, the OCP of 904L was about 100 mV higher in the solution with 5 g/l Fe^{3+} than with 0.5 g/l Fe^{3+}. The lowest OCP values were detected in Solution 2 (5 g/l Cu^{2+}), again similarly to the redox potential, but the difference to Solution 3 (5 g/l Fe^{2+}) was minimal.

3.2. Immersion crevice corrosion tests and characterization of the attack

The measured mass losses are presented in Fig. 2 for flat and serrated crevice formers. 904L experienced measurable mass loss in all test environments when tested with flat crevice formers but only in the two ferric iron containing solutions when serrated crevice formers were employed. The flat crevice former generated more demanding crevice conditions. For 2205, evident mass loss was seen only in the two ferric iron containing solutions (Solutions 1 and 4). For 2507, no mass loss was detected in any of the test solutions. Based on the appearance of the sample surfaces observed with stereomicroscopy, no uniform corrosion occurred. This is consistent with the iso-corrosion curves and corrosion data for uniform corrosion given in [29].

Photographs of the specimens are shown in Fig. 3. Crevice corrosion was evident in the specimens of grade 904L in the ferric iron containing solutions (Solutions 1 and 4) and in the

copper containing solution (Solution 2). In the solution with ferrous iron (Solution 3), no crevice corrosion was found, but pitting corrosion was detected in one passivated edge (Figs. 4a and b), thus explaining the high mass loss in the absence of crevice corrosion. The specimens of test material 2205 experienced crevice corrosion only in the ferric iron containing solutions (Solutions 1 and 4). Additionally, edge corrosion was apparent in the solution with 5 g/l ferric iron (Solution 1, Fig. 4c). In the case of specimens of 2507, no signs of corrosion attack were observed. Table 6 provides a summary of the observed forms of corrosion.

Figure 3 enables some observations on the characteristics of the crevice corrosion attack using the float crevice formers, which produced more severe crevice corrosion attack in the specimens than the serrated ones. In 904L, the extent of attack was greatest near the edges of the crevice, but otherwise the attack was relatively uniformly spread underneath the crevice former. In 2205, the attack within the covered areas was spread much more unevenly than in the case of 904L, with the materials degradation occasionally following microstructural features of the material. These observations are supported by SEM investigations. In 904L (Fig. 5), the edge areas around the crevice formers were most heavily attacked, with areas around the external rather than internal periphery of the circular crevice former showing the heaviest attack (Figs. 5a and b). Cross-sectional examinations revealed that the attack was occasionally spread laterally in the material (Figs. 5c and d). In 2205 (Figs. 6 and 7), degradation of the material occurred more unevenly in the areas under the crevice former than in 904L, with only very little attack in some areas, but evidently more material loss in some other locations. Detailed investigations systematically revealed selective dissolution (Figs. 6c and d, 7c and d). Based on EBSD characterization, austenite was primarily attacked, whereas the areas of the ferrite phase were retained intact (Fig. 8). EDS analyses taken from distinct areas of austenite and ferrite (Fig. 8a, Table 7) disclosed compositional differences. According to the analyses in Table 7, austenite was relatively enriched in nickel and manganese, whereas ferrite contained relatively more chromium, molybdenum and silicon. When converted into PREN-values, that of austenite (31 in grade 2205, 38 in grade 2507)

was lower than that of ferrite (37 in grade 2205, 44 in grade 2507). The effect of nitrogen was excluded from these calculations as its determination with EDS is associated with uncertainty. If it is assumed that the ferrite phase contains the saturation amount of 0.05% N and the rest of N is assigned to the austenite phase [30], the PREN-value of austenite will increase only by 2 units with respect to that of ferrite, still demonstrating a substantial difference in PREN-values between the two phases.

The measured mass loss did not systematically correlate with the extent of crevice corrosion in the specimens of 904L and 2205 due to the fact that occasionally other corrosion mechanisms related to the edges of the samples were active, too (Fig. 4). For example, in Solution 1 (5 g/l Fe^{3+}), the depth of the crevice corrosion attack was measured to be 2.3 mm in 904L and 0.3 mm in 2205. Similarly, in Solution 4 (0.5 g/l Fe^{3+}), the attack had progressed to the depths of 1.5 mm and 0.25 mm. In other words, crevice corrosion was more severe for 904L than for 2205, although the mass losses in the case of Solution 1 (5 g/l Fe^{3+}) predict the opposite.

3.3. Electrochemical measurements

The test solutions used in the electrochemical measurements are shown in Table 8. Cyclic polarization curves for the three stainless steel grades in the base solution containing 50 g/l H_2SO_4 and 1 g/l Cl^- are shown in Fig. 9. Slight differences were observed between the test materials in the critical values for current density, i_{pp}, and potential, E_{pp}, to reach the passive state. The highest i_{pp} and E_{pp} values, 0.6 mA/cm^2 and -170 mV, respectively, were detected for 904L. In turn, the lowest i_{pp}, 0.01 mA/cm^2, was obtained for grade 2507, while the lowest E_{pp}, -230 mV, was obtained for grade 2205. Concerning the tendency to crevice corrosion, these results mean that the active peak may be most easily reached in the case of grade 904L, followed by grade 2205. In the case of 2507, the active region barely existed. However, once the passive state was reached, the passive current density i_{pass} was relatively equal in all cases, ranging from 2 to 5 μA/cm^2. In the case of

duplex steel grade 2205, a shoulder was detected in the beginning of the passive region around 0 mV. This can relate to the fact that the austenite and ferrite phases show active dissolution at different potentials [30, 31]. In contrast, for 2507, no such shoulder in the passive region of the polarisation curve could be seen. For all three test materials, transpassive dissolution started at the same potential, at about 900 mV vs. Ag/AgCl. None of the measured curves included a hysteresis loop between the forward and reverse scans that indicates tendency to pitting and crevice corrosion.

The influence of three key solution constituents, the oxidizing ion Fe^{3+} content, the chloride ion Cl^- content, and the sulfate ion SO_4^{2-} content on the ratio of the activities of chloride and sulfate ions are given in Table 8. Their influence on the polarisation curves is shown in Fig. 10 using grade 904L as an example. The addition of Fe^{3+} decreased the activity ratio between chlorides and sulfates (Table 8) and shifted the corrosion potential upwards (Fig. 10a). The active/passive transition was not resolved in the polarization curves with Fe^{3+} additions, probably because the transition was below the OCP and hidden by the cathodic part of the curve. The corrosion potential values obtained in the cyclic polarization tests agreed well with the values obtained in the OCP measurements. The increase in chloride content, in contrast, raised the activity ratios between chlorides and sulfates and brought clear changes in the behaviour of grade 904L, particularly at chloride contents of 5 g/l and higher. The curves in the absence of chlorides and at the chloride content of 1 g/l were almost equal, but further increase in the chloride content caused a dramatic increase in i_{pp} and i_{pass} and pitting corrosion occurred instead of transpassive dissolution. At the chloride content of 1 g/l, i_{pp} was 0.6 mA/cm^2, but increased first to 2.4 and then further to 5.3 mA/cm^2 along the increasing chloride content. The corresponding increase in i_{pass} was higher than in i_{pp}, with a rise by more than one order of magnitude, while increasing the chloride content from 1 to 5 g/l and even slightly more, when reaching the chloride content of 10 g/l. With the chloride contents of 5 g/l and 10 g/l, 904L exhibited pitting corrosion at high potentials instead of transpassive dissolution. The pitting potential in the 5 g/l chloride solution was 380 mV and in the

10 g/l chloride solution it was further lowered to 200 mV. The addition of sulfate, Fig. 10c, slightly decreased the i_{pp} needed for passivation, to the same level as in the base solution (50 g/l H_2SO_4, 1 g/l Cl^-), evidently due to the relatively equal ratio of activities between chlorides and sulfates, Table 8. Simultaneously, i_{pass} was lowered by more than one order of magnitude and the pitting potential was increased by more than 400 mV, consistent with the observations in the base solution (50 g/l H_2SO_4, 1 g/l Cl^-).

Keeping in mind the dramatic changes in the behaviour of 904L at the chloride concentration of 5 g/l and the fact that the crevice solutions typically enrich in chlorides, polarization curves for all three test materials were determined at this chloride content (Fig. 11). Here, dissimilarities in the behaviour were evident between the alloys. Grade 2507 was least influenced by the high chloride content of the solution, with the forward curve being almost identical to that detected at the lower chloride content (Fig. 9) despite a more distinct active-passive transition, and the formation of a hysteresis loop between the forward and reverse scans at the high potentials. The measured hysteresis loop was, however, closed in the beginning of the reverse scan but opened at slightly lower potentials. This type of behaviour is not a manifestation of pitting corrosion but is rather due to the occurrence of crevice corrosion in the sample. Repassivation was detected for 2507 below the potential of about 500 mV vs. Ag/AgCl. During the forward scan, the higher chloride content brought a shoulder to the polarization curve at about -80 mV which was not seen with 1 g/l chloride but has been observed for super duplex stainless steels, e.g. in 3M HCl [30].

Grades 904L and 2205 behaved in a relatively consistent manner, and the passive currents were the same for both grades. Both grades also showed a clear active peak. In the case of grade 2205, the active peak showed a bimodal shape suggesting that the austenite and ferrite phases dissolve at different potentials. In 4M H_2SO_4 + 1M HCl, active dissolution of the ferrite phase was reported to occur at E_{corr} + 50 mV and that of the austenite phase at somewhat higher potential of E_{corr} + 150 mV [32]. Based on the similarity of the environments this suggests that the austenite phase

dissolves at a slightly higher potential than the ferrite phase, enabling a smaller IR drop to cause the dissolution of austenite in a crevice.

4. Discussion

4.1. Effect of sulfate ions on localized corrosion

It is well established that pitting corrosion of stainless steels occurs when the corrosion potential exceeds a critical value E_{pit} in the passive range of the polarization curve. E_{pit} decreases with the logarithm of the chloride concentration or activity [33]. In addition, pH and temperature exert some influence on the critical pitting corrosion temperature. Sulfate ions inhibit pitting corrosion owing to the competitive absorption of chloride and sulfate ions [34], and anions with the highest charge will be preferentially accumulated at the metal-solution interface [4]. Similarly, the presence of sulfates has been shown to inhibit crevice corrosion. E.g., Brossia and Kelly [35] demonstrated the effect for austenitic 304 stainless steel in neutral chloride solutions. They stated that the inhibition of crevice corrosion was primarily due to the competitive migration and/or absorption between SO_4^{2-} and Cl^-. A similar conclusion is made in ref. [36], explaining the delay in achieving the critical concentration of chlorides in the crevice. Pardo et el. [37] observed that the critical pitting and crevice corrosion temperatures of superduplex and superaustenitic stainless steel grades increased when the test solution was acidified with sulfuric acid.

When our immersion test results are compared to the results from immersion tests conducted for welded specimens in a relatively similar environment, they are well in line. Ekman [2] immersed creviced stainless steel samples in 10% H_2SO_4 with 0.7 g/l Cl^-, 5 g/l Fe^{3+} and 4 g/l Cu^{2+} at 90ºC and observed that 904L showed pitting corrosion in the heat-affected zone, but 2205 and 2507 were free from corrosion. In the solution with 1% H_2SO_4, 5 g/l Fe^{3+} and 4 g/l Cu^{2+} with a chloride concentration of 1 g/l Cl^- and at a slightly higher temperature, 98ºC, 904L and 2205 displayed

uniform, pitting and crevice corrosion, but 2507 showed only minor uniform corrosion and pitting corrosion in the weld.

Comparing the results to investigations carried out at higher temperatures and relatively small chloride concentrations, the beneficial effect of sulfates can be noted. The experimental and modelling results of Anderko et al. [38] give for grade 2205 a repassivation potential of +30 mV vs. Ag/AgCl at 95ºC with similar chloride activities as in our test solutions. This low value suggests that crevice and/or pitting corrosion should have occurred in all our test environments, which was not the case for grade 2205. For a corrosion-resistant high-nickel alloy Alloy 825, a repassivation potential of 50±100 mV vs. Ag/AgCl was obtained in 1 g/l Cl^- at 95ºC [18], which is lower than those seen in our tests for any of the steel grades.

When the test solutions are compared to each other, it can be noted that they are fairly similar with respect to the ratios between the activities of chlorides and sulfates. Then the primary factor that governs the occurrence of crevice corrosion is the OCP of the material. Considering the IR drop mechanism for crevice corrosion, Equation 2 states that the higher the surface potential, the larger IR drop is required to initiate crevice corrosion. However, when the polarization curves are investigated it can be seen, e.g. in Fig. 10b, that the higher surface potential translates into a higher current which increases the IR drop. The effect of increasing IR surpasses the effect of increasing $\Delta\emptyset^*$ and consequently, the critical condition is more readily attained in solutions with higher oxidizing power, such as in Fe^{3+}-containing solutions, compared to the solutions with a lower oxidizing power, such as Cu^{2+}-containing solutions.

4.2 Occurrence of crevice corrosion and implications of the IR drop mechanism

The maximum loss of thickness in grade 904L was detected at the distance of approximately 0.5-1.5 mm inwards from the crevice mouth (Fig. 3). It is well established from microelectrode experiments, that corrosion damage spreads after initiation both towards the mouth of the crevice but also inwards [12]. In duplex steel grades 2205 and 2507 the loss of thickness was homogeneous under the crevice former. The activation by IR drop mechanisms explains the differences in the crevice morphology, given that grade 904L featured the lowest PREN (with possibility of pitting within the crevice) and that the duplex grades underwent preferential dissolution of the phase with a lower PREN. When examining the polarization curves measured in the bulk solution (Fig. 10) it can be seen that the required IR drop for crevice corrosion to occur in such a solution is very high, of the order 800 mV in the case of 5 g/l ferric iron (Solution 1) and almost 700 mV in the case of 0.5 g/l ferric iron (Solution 4). The required IR drop is by far higher than typically measured, e.g., by microelectrode arrays [11]. Consequently, it can be expected that the materials are spontaneously passive in the bulk solution, but the potential drop associated with the critical crevice dimensions (the critical depth and the width of the crevice) brings them into the active region. Indeed, as stated by Engelhardt and Macdonald [39], the rate of anodic dissolution of the metal determines the depth of attack inside the corroding crevices.

Typically it is thought that the acidification of the solution and the migration of negatively charged chloride anions to balance the effect of the positively charged metal cations are responsible for the creation of an aggressive crevice solution. The mobility of chloride ion is roughly twice that of the sulfate ion (D_{Cl^-} = 2.03·10^{-9} m^2/s and $D_{SO_4^{2-}}$ = 1.07·10^{-9} m^2/s at room temperature, D_{Cl^-} = 6.57·10^{-9} m^2/s and $D_{SO_4^{2-}}$ = 3.73·10^{-9} m^2/s at 96°C)[40], thus it may be expected that chloride is the ion moving preferentially to the crevice area. In our study, this is not as straightforward as the solution is initially highly acidic (pH 0.5) and contains a high amount of negatively charged sulfate ions in the bulk solution and also inside the crevice. Actually, the given explanation holds primarily for the

acidification model, whereas for materials exhibiting active-passive behaviour, the IR drop model explains the crevice attack even in the complete absence of acidification and chloride accumulation (yet these are not completely excluded). The IR drop model is therefore well suited for the description of the studied three stainless steel grades in the examined leaching environment, particularly as the pH-values are initially so low that minor changes in the H^+ concentration do not cause noteworthy changes in pH.

The application of the IR drop model has some implications in the interpretation of the polarization data, as the active-passive transformation and the influence of various ions (oxidizing species, chlorides, sulfates) on it are in the key role. As shown in Fig. 10, the addition of Fe^{3+} shifts the OCP radically upwards, hiding the clear active-passive transition from the polarisation curve of grade 904L. The increase in the chloride content raises the chloride activity and increases the active current densities. The addition of sulfate (45 g/l) restores the ratio of activities between chlorides and sulfates to the same level as in the base solution (50 g/l H_2SO_4, 1 g/l Cl^-) and brings the current density values within the active area to the same level as in the base solution. However, due to the fact that the ionic species take part in the reactions through their activities which are determined by the equilibrium chemistry of the solution, the influence of chloride additions on the ratio of activities between chlorides and sulfates, and on the corrosion behaviour of the test materials is much stronger than those of sulfates. Therefore, when negatively charged species are attracted into the crevice, the corrosion effects of chlorides dominate those of sulfates. Considering the greater mobility of chloride ion as that of sulfate ion, such situation is highly probable.

4.3 Effect of the metal cations

The presence of the oxidizing ions: ferric or cupric ions may influence the localized corrosion of stainless steels in two ways. First, their presence increases the corrosion potential of the material to various extents. Second, the ions interact with the other constituents of the occluded cell

solution. The addition of ferric or ferrous ions changes the concentration of ions naturally released from stainless steels during corrosion. In the case of the duplex stainless steels, the presence of copper brings a new ion into the bulk and occluded cell solutions as they are not alloyed with copper. Conversely, 904L is alloyed with copper. Under neutral conditions copper has not been detected to enrich into the crevice corroded surface [41]. Under highly acidic conditions the enrichment can, however, be expected as copper is alloyed to improve uniform corrosion resistance in sulfuric acid media. The concentrations that can enter through dissolution into the occluded cell solution can still be minor compared to the concentration in the bulk solution, 5 g/l. Other constituents of the occluded cell solution can be thought to be nickel and chromium when allowing for congruent dissolution.

Considering oxidation capacity, it is well known that a higher potential conveys to a more extensive local damage. In this respect it is expected that the solutions with the ferric ions generate the most severe crevice corrosion damage, as indeed was observed for grades 904L and 2205. However, the redox potentials and the ratio of the activities of chlorides and sulfates in the two remaining solutions: the one with copper ions (Solution 2) and the other with ferrous ions (Solution 3) were similar, but crevice corrosion was observed only in 904L in the copper-containing solution (Solution 2). This suggests that the ion-ion interactions in the occluded cell solution generate more aggressive conditions in the presence of copper ions than in the presence of ferrous ions. One possible explanation for the differences in the occurrence of crevice corrosion in Fe^{2+}- and Cu^{2+}-containing solutions, when the ratios of the activities of chlorides and sulfates and the OCP values are similar, may relate to the difference in the complexing tendency of Fe^{2+} and Cu^{2+}. In aqueous solutions, metal ions make complexes with water molecules. Chloride ions can substitute one or several water molecules depending on the reaction constants, thus also chloride may act as a ligand for metal ion co-ordinates. For Fe^{2+}, only one water ligand can be substituted by chloride giving a formation constant of $\log K_1 = 0.36$ [42]. For copper, the formation constant for the first water substitution by chloride is $\log K_1 = 0.1$ and the second cumulative formation constant $\log K_2 =$

-0.6. This indicates that the complex of Fe^{2+} and Cl^- is more stable than that between Cu^{2+} and Cl^-. Then one may expect that in the Fe^{2+}-containing solution there are less free chloride ions that can interact with the passive film of the stainless steel, and this reduces the crevice corrosion tendency, which was seen experimentally.

4.4. Comparison between the stainless steel grades

The PREN-value predicts the resistance of a stainless steel to localized corrosion attack. The obtained results proved that PREN of 43 in the case of grade 2507 was high enough to avoid crevice corrosion in the aggressive environment containing 50 g/l H_2SO_4 and 1 g/l Cl^- despite the presence of oxidizing ions. Although the oxidizing ions were demonstrated to ennoble the corrosion potential of the materials significantly, the passive region detected for 2507 was so wide that the passive-active transition was clearly prevented. Even in the concentrated chloride solution, the passivity was preserved well above the redox potential of the Fe^{3+} containing test solutions.

In the case of grades 904L and 2205, the PREN-values were almost equal, but there were differences in the degradation mechanism due to microstructural dissimilarities. With respect to the electrochemical response, the two alloys behaved relatively consistently in the solution containing 50 g/l H_2SO_4 and 1 g/l Cl^- and in the concentrated chloride solution. Minor differences in the parameters enabling the active-passive transformation and the initiation of pitting corrosion were detected between the alloys and these may have some role in the observations between the four test solutions. However, what is important with regard to the crevice corrosion susceptibility is the significant dependence of the behaviour of these two materials on the chloride concentration, as demonstrated in Figs. 9 and 11. For both materials, the passive region shrinks and the passive current i_{pass} increases with increasing chloride content. In the case of austenitic alloy 904L, the most severe damage was detected within some distance from the crevice mouth, which is consistent with the current understanding of the damage evolution [43,44]. Indeed, the external

periphery of the crevice former was surrounded by a larger cathodic area than the inner periphery, explaining the location of the damage near the crevice mouth.

In the case of duplex steel grade 2205, the presence of the two phases with dissimilar resistance to corrosion, evaluated on the basis of the PREN-values, explains the uniform lateral spreading of the corrosion attack within the crevice. As the austenite phase has a much lower PREN-value than that of the overall bulk material, and active dissolution of austenite occurs at slightly higher potentials than that of ferrite, i.e., a smaller IR drop is required to dissolve the austenite phase, the attack proceeds along the evenly distributed austenite areas. Although the experimental PREN-values rely on the EDS spot analyses where part of the collected information may come from the surroundings, the PREN-values provide enough relative information to enable the comparison, even though they are not absolute PREN-values. Similarly for 2507 austenite was the phase with the lower PREN value thus more prone to localized corrosion.

5. Conclusions

The investigation of crevice corrosion behaviour of three stainless steel grades: 904L, 2205 and 2507, in a leaching environment based on H_2SO_4 containing chlorides and oxidizing ions enables the following conclusions to be made:

1) The extent and nature of crevice corrosion attack varies between the steel grades of nominally identical PREN-values (austenitic 904L and duplex 2205 have PREN-values 34 and 35, respectively) and between the solutions with dissimilar chemistries (ratio of activities of chlorides and sulfates, type of oxidizing ions). The duplex steel grade 2507 (PREN 43) is not susceptible to crevice corrosion under any of the studied conditions.

2) Grade 904L undergoes the most severe crevice corrosion among the studied alloys, with the corrosion attack being evident in the solutions containing ferric iron (5 and 0.5 g/l Fe^{3+}) and cupric ions (5 g/l Cu^{2+}), together with chlorides (1 g/l Cl^{-}).
3) In the duplex stainless steel 2205, crevice corrosion is evident in the solutions containing ferric iron (5 and 0.5 g/l Fe^{3+}). Here, the ratio of activities of chlorides and sulfates is particularly important with respect to the extent of corrosion attack, with a lower ratio leading to greater material loss. The austenite and ferrite phases undergo dissolution at different rates, austenite phase being preferentially attacked in the studied leaching environments.

4) The influence of enrichment of chlorides and sulfates in the crevice on the behaviour of the test materials is demonstrated through anodic polarisation measurements in concentrated chloride solutions. Although the passive region is significantly influenced by the concentration of these ions, also the active peak shifts to higher (increase in chloride content) or lower (increase in sulfate content) current densities upon altering their amount and ratio of activities.

Acknowledgements

The work was carried out within the Digital, Internet, Materials & Engineering Co-Creation platform (DIMECC Oy) and its Breakthrough Steels and Applications (BSA) program. We gratefully acknowledge the financial support from the Finnish Funding Agency for Technology and Innovation (Tekes) and participating companies. VTT Technical Research Centre of Finland Ltd is also acknowledged for funding. At VTT, the technical staff, particularly Tuomo Kinnunen, is thanked for conducting the electrochemical measurements.

References

1. H.R. Watling, Chalcopyrite hydrometallurgy at atmospheric pressure: 1. Review of acidic sulfate, sulfate-chloride and sulfate-nitrate process options, Hydrometallurgy, Vol. 140, 2013, 163-180.

2. S. Ekman, E. Torsner, Special stainless steel grades for the hydrometallurgical industry. Proceedings of Copper 2010, Hamburg, Germany, 1857-1870.

3. Z. Szklarska-Smialowska, Pitting and Crevice Corrosion. NACE International, Houston, USA, 2005.

4. J.R. Galvele, Transport processes and the mechanism of pitting of metals., Journal of the Electrochemical Society, Vol. 123, No. 4, 1976, 464-474.

5. H.W. Pickering, Important early developments and current understanding of the IR mechanism of localized corrosion. Journal of the Electrochemical Society, Vol. 150, No. 5, 2003, K1-K3.

6. B.A. Kehler, J.R. Scully, Role of metastable pitting in crevices on crevice corrosion stabilization in Alloy 625 and 22, Corrosion, Vol. 61, No. 7, 2005, 665-684.

7. N.J. Laycock, J. Stewart, R.C. Newman, The initiation of crevice corrosion in stainless steels. Corrosion Science, Vol. 39, No. 10-11, 1997, 1791-1809.

8. M.I. Abdulsalam, Behavior of crevice corrosion in iron. Corrosion Science, Vol. 47, 2005, 1336-1351.

9. M.I. Abdulsalam, H.W. Pickering, Effect of applied potential on the potential and current distributions within crevices in pure nickel. Corrosion Science, Vol. 41, 1999, 351-372.

10. A.M. Al-Zahrani, H.W. Pickering, IR voltage switch in delayed crevice corrosion and active peak formation using repassivation-type scan. Electrochimica Acta, Vol. 50, 2005, 3420-3435.

11. N. Sridhar, D.S. Dunn, Effect of applied potential on changes in solution chemistry inside crevices of type 304L stainless steel and alloy 825. Corrosion, Vol. 50, No. 11, 1994, 857-872.

12. F. Bocher, F. Presuel-Moreno, J.R. Scully, Investigation of crevice corrosion of AISI 316 stainless steel compared to Ni-Cr-Mo alloys using coupled multielectrode arrays. Journal of the Electrochemical Society, Vol. 155, No. 5, 2008, C256-C268.

13. K. Cho, H.W. Pickering, The role of chloride ions in the IR>IR* criterion for crevice corrosion of iron. Journal of the Electrochemical Society, Vol. 138, No. 10, 1991, L56-L58.

14. T. Kaji, T. Sekai, I. Muto, Y. Sugawara, N. Hara, Visualization of pH and pCl distributions: initiation and propagation criteria for crevice corrosion in stainless steel. Journal of the Electrochemical Society, Vol. 159, No. 7, 2012, C289-C297.

15. H.W. Pickering, On the roles of corrosion products in local processes. Corrosion, Vol. 42, No. 3, 1986, 125-140.

16. K. Cho, M.I. Abdulsalam, H.W. Pickering, The effect of electrolyte properties on the mechanism of crevice corrosion in pure iron. Journal of the Electrochemical Society, Vol. 145, No. 6, 1998, 1862-1869.

17. M.I. Abdulsalam, H. Alghamdi, S.T. Arab, Y.T. Al-Janabi, Susceptibility of superaustenitic stainless steel alloys to crevice corrosion in chloride solutions. Proceedings of European Corrosion Congress 2011, EuroCorr2011, Stockholm, Sweden, 2011.

18. D.S. Dunn, G.A. Cragnolino, N. Sridhar, An electrochemical approach to predicting long-term localized corrosion of corrosion resistant high-level waste container materials. Corrosion, Vol. 56, No. 1, 2000, 90-104.

19. F. Bocher, R. Huang, J.R. Scully, Prediction of critical crevice potentials for Ni-Cr-Mo alloys in simulated crevice solutions as a function of molybdenum content. Corrosion, Vol. 66, No. 5, 2010, 055002-1 – 055002-15.

20. M.A. Rodriguez, R.M. Carranza, R.B. Rebak, Effect of potential on crevice corrosion kinetics of alloy 22. Corrosion, Vol. 66, No. 1, 2010, 015007-1-015007-14.

21. U. Steinsmo, T. Rogne, J.M. Drugli, P.O. Gartland, Critical crevice temperature for high-alloyed stainless steels in chlorinated seawater applications. Corrosion, Vol. 53, No. 1, 1997, 26-32.

22. D. Han, Y. Jiang, B. Deng, L. Zhang, J, Gao, H. Tan, J. Li, Detecting critical crevice temperature for duplex stainless steels in chloride solutions. Corrosion, Vol- 67, No. 2, 025004-1 – 025004-7.

23. D. Han, Y. Jiang, C. Shi, Z. Ji, J. Li, Influence of the microstructure and alloying element on the polarization behavior within the crevice of UNS S32304 duplex stainless steel. Corrosion Science, Vol. 53, 2011, 3796-3804.

24. Y.Z. Yang, Y.M. Jiang, J. Li, In situ investigation of crevice corrosion on UNS S32101 duplex stainless steel in sodium chloride. Corrosion Science, Vol. 76, 2013, 163-169.

25. J.N. Al-Khamis, H.W. Pickering, IR mechanism of crevice corrosion for Alloy T-2205 duplex stainless steel in acidic-chloride media. Journal of the Electrochemical Society, Vol. 148, No. 8, 2001, B314-B321.

26. HSC Software, version 8.1.

27. H. Sippola, Thermodynamic modelling of aqueous sulfuric acid. PhD thesis, Department of Materials Science and Engineering, Aalto University, Espoo, Finland, 2015.

28. G. Yue, L. Zhao, O.G. Olvera, E. Asselin, Speciation of the H_2SO_4-$Fe_2(SO_4)_3$-$FeSO^{4-}$ H_2O system and development of an expression to predict the redox potential of the Fe^{3+}/Fe^{2+} couple up to 150ºC. Hydrometallurgy, Vol. 147-148, 2014, 196-209.

29. Corrosion Handbook, Outokumpu Stainless, 10th ed. 2009.

30. R.A. Perren, T.A. Suter, P.J. Uggowitzer, L. Weber, R. Magdowski, H. Böhmi, M.O. Speidel, Corrosion resistance of super duplex stainless steels in chloride ion

containing environments: investigation by means of a new microelectrochemical method: I. Precipitation-free states. Corrosion Science, Vol. 43, 2001, 707-726.

31. E. Symniotis, Galvanic effects on the active dissolution of duplex stainless steels. Corrosion, Vol. 46, No. 1, 1990, 2-12.

32. M. Feminia, J. Pan, C. Leygraf, P. Luukkonen, In situ study of selective dissolution of duplex stainless steel 2205 by electrochemical scanning tunneling microscopy. Corrosion Science, Vol. 43, 2001, 1939-1952.

33. H.P. Leckie, H.H. Uhlig, Environmental factors affecting the critical potential for pitting in 18-8 stainless steel. Journal of the Electrochemical Society, Vol. 113, 1966, 1261-1267.

34. S.-I. Pyun, S.-M. Moon, The inhibition mechanism of pitting corrosion of pure aluminium by nitrate and sulphate ions in neutral chloride solution. Journal of Solid State Electrochemistry Vol. 3, 1999, 331-336.

35. C.S. Brossia, R.G. Kelly, Influence of alloy sulfur content and bulk electrolyte composition on crevice corrosion mitigation of austenitic stainless steel. Corrosion, Vol. 54, No. 2, 1998, 145-154.

36. E.A. Abd El Meguid, A.A. Abd El Latif, Electrochemical and SEM study on Type 254 SMO stainless steel in chloride solutions. Corrosion Science, Vol. 46, 2004, 2431-2444.

37. A. Pardo, E. Otero, M.C. Merino, M.D. Lopéz, M.V. Utrilla, F. Moreno, Influence of pH and chloride concentration on the pitting and crevice corrosion behavior of high-alloy stainless steel. Corrosion, Vol. 56, No. 4, 2000, 411-418.

38. A. Anderko, N. Sridhar, M.A. Jakab, G. Tormonen, A general model for the repassivation potential as a function of multiple aqueous species. 2. Effect of oxyanions on localized corrosion of Fe-Ni-Cr-Mo-W-n alloys. Corrosion Science, Vol. 50, 2008, 3628-3647.

39. G.E. Engelhardt, D.D. Macdonald, Possible distribution of potential and corrosion current density inside corroding crevices. Electrochimica Acta, Vol. 65, 2012, 266-274.

40. S.-K. Lee, The coupled environment models for localized corrosions; Crevice corrosion and stress corrosion cracking, Dissertation of Pennsylvania State University, August, 2013.

41. S. Zakipour, C. Leygraf, Surface composition of stainless steel during propagation of crevice corrosion. Corrosion, Vol. 37, No. 1, 1981, 21-28.

39. J.A. Dean, Lange's Handbook of Chemistry. 14th edition, McGraw-Hill Inc. New York, 8.83-8.97.

43. G.F. Kennell, R.W. Evitts, Crevice corrosion cathodic reactions and crevice scaling laws. Electrochimica Acta, Vol. 54, 2009, 4696-4703.

44. W. Sun, L. Wang, T. Wu, G. Liu, An arbitrary Lagrarian-Eulerian model for modelling the time-dependent evolution of crevice corrosion. Corrosion Science, Vol. 78, 2014, 233-243.

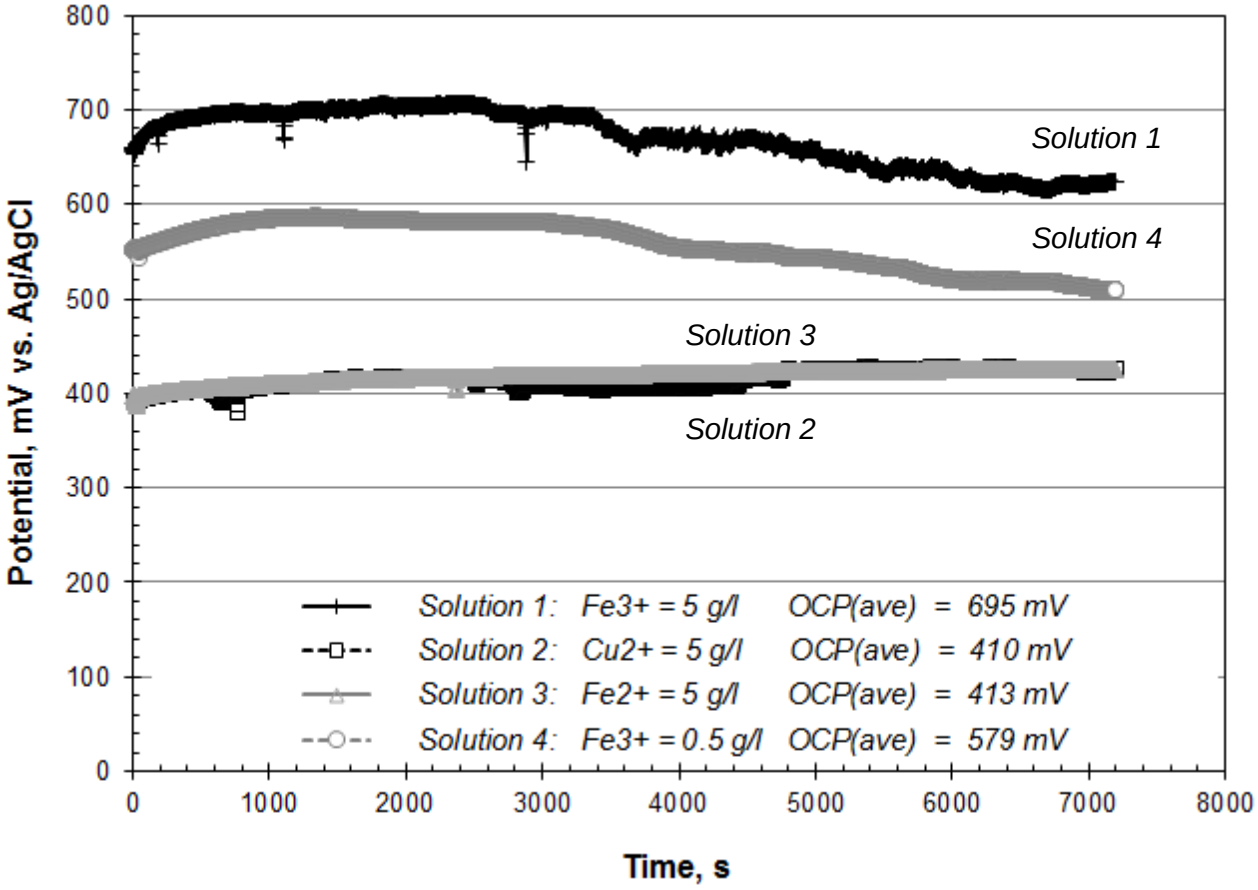

Figure 1. Open circuit potential records for the specimens of grade 904L in the test solutions during the first 2 h of the experiment.

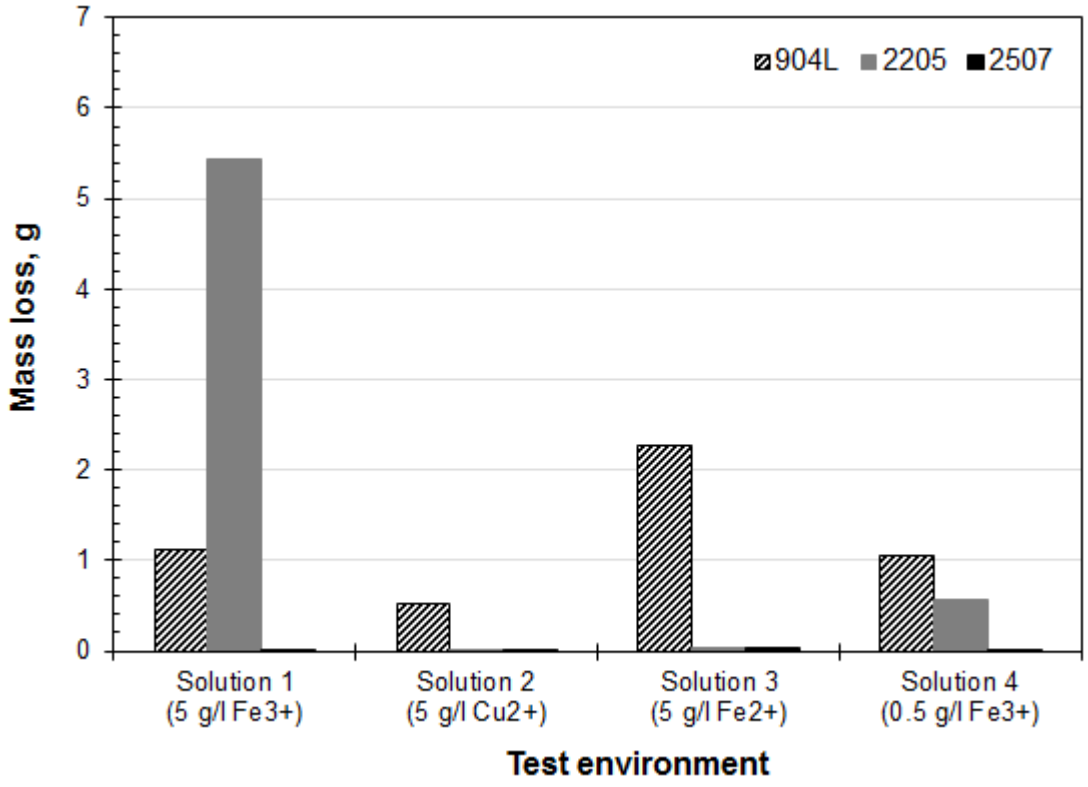

a)

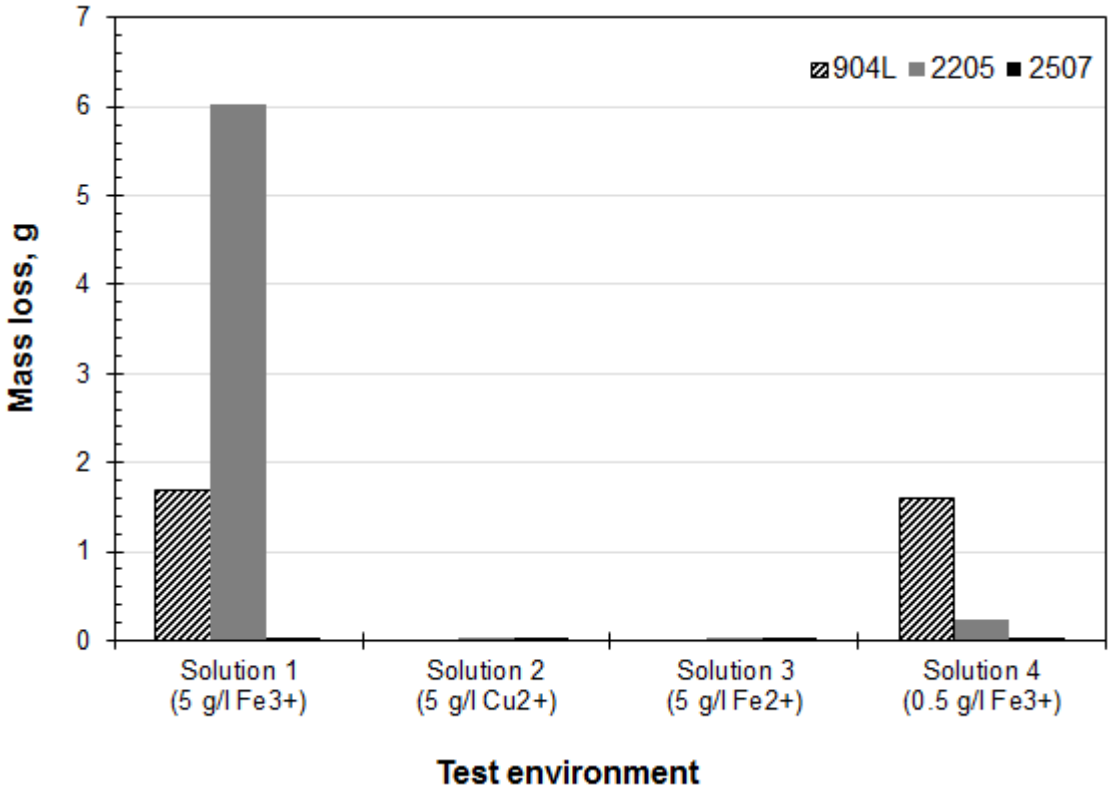

b)

Figure 2. *Measured mass loss of the specimens of each test material using the two types of crevice formers. a) Crevice former with flat surfaces. b) Crevice former with serrated surfaces.*

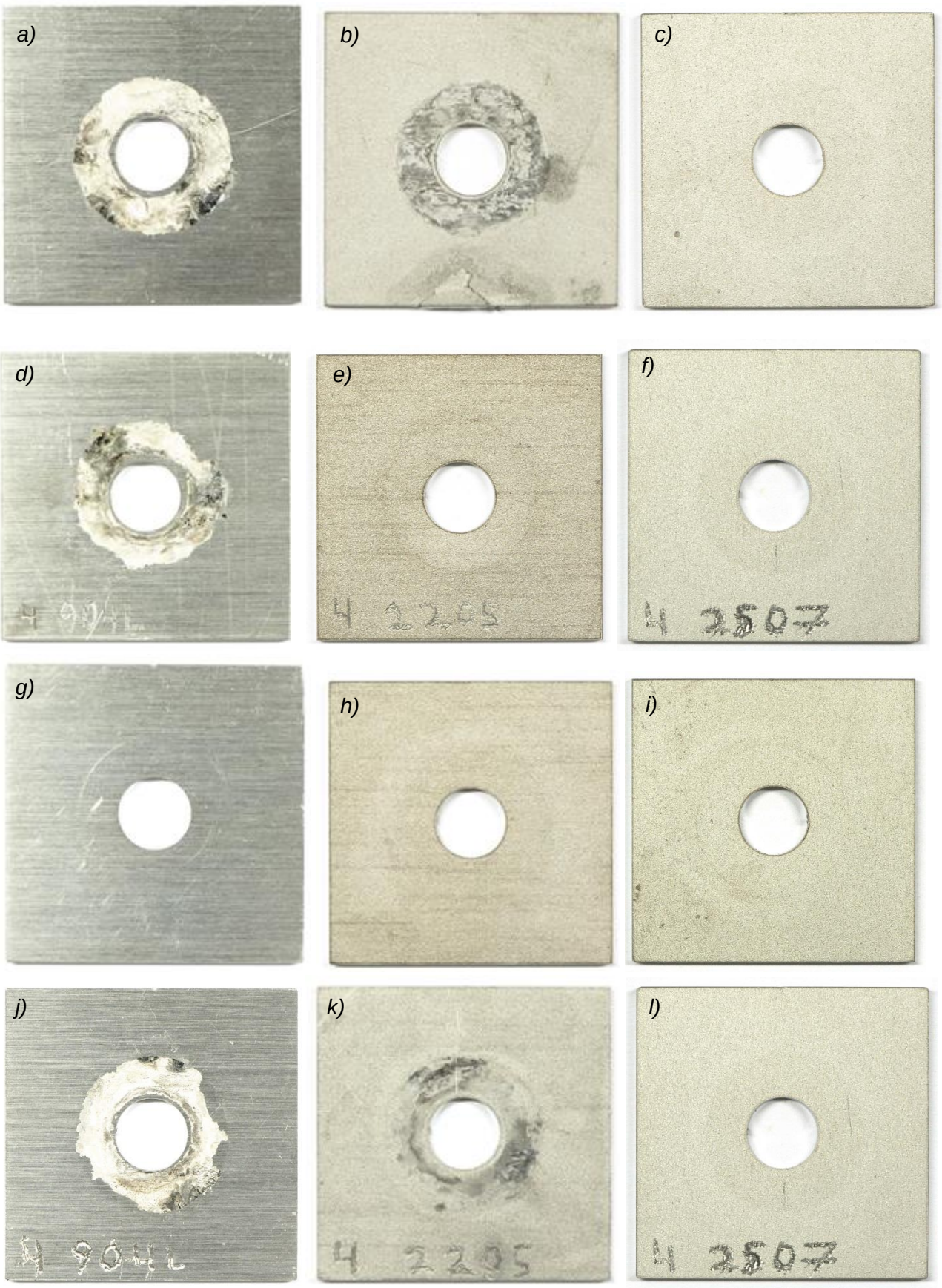

Figure 3. Photographs of the specimens after the testing using flat crevice formers. a-c) Solution 1. d-f) Solution 2. g-i) Solution 3. j-l) Solution 4. The images on the left (a, d, g, j) are of grade 904L, the images in the middle column (b, e, h, k) are of grade 2205 and those on the right (c, f, I, l) are of grade 2507.

a)

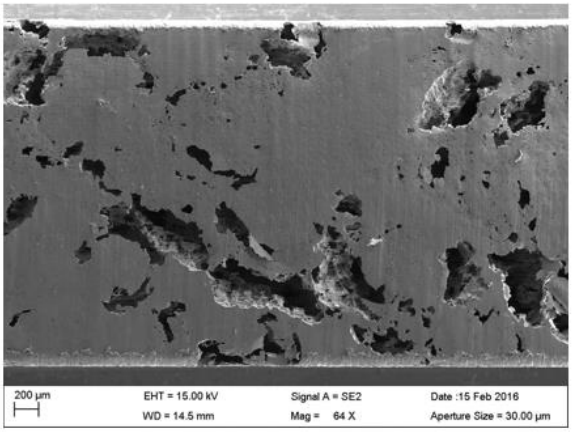

b)

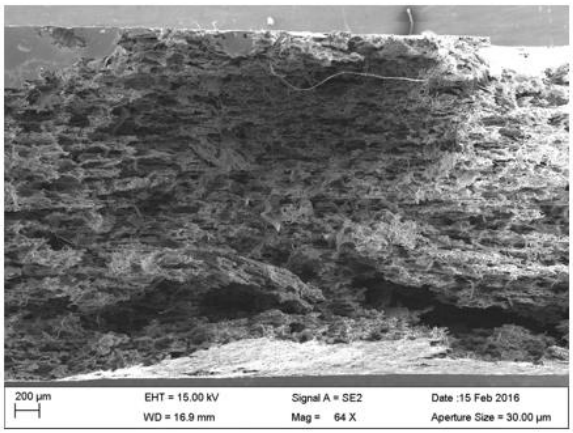

c)

Figure 4. *a) A photograph and b, c) SEM images showing the pitting corrosion in the passivated edges of the specimens. a, b) Grade 904L in Solution 3 (Fe^{2+} 5 g/l). c) Grade 2205 in Solution 1 (Fe^{3+} 5 g/l). Photographs are from experiments employing flat crevice formers.*

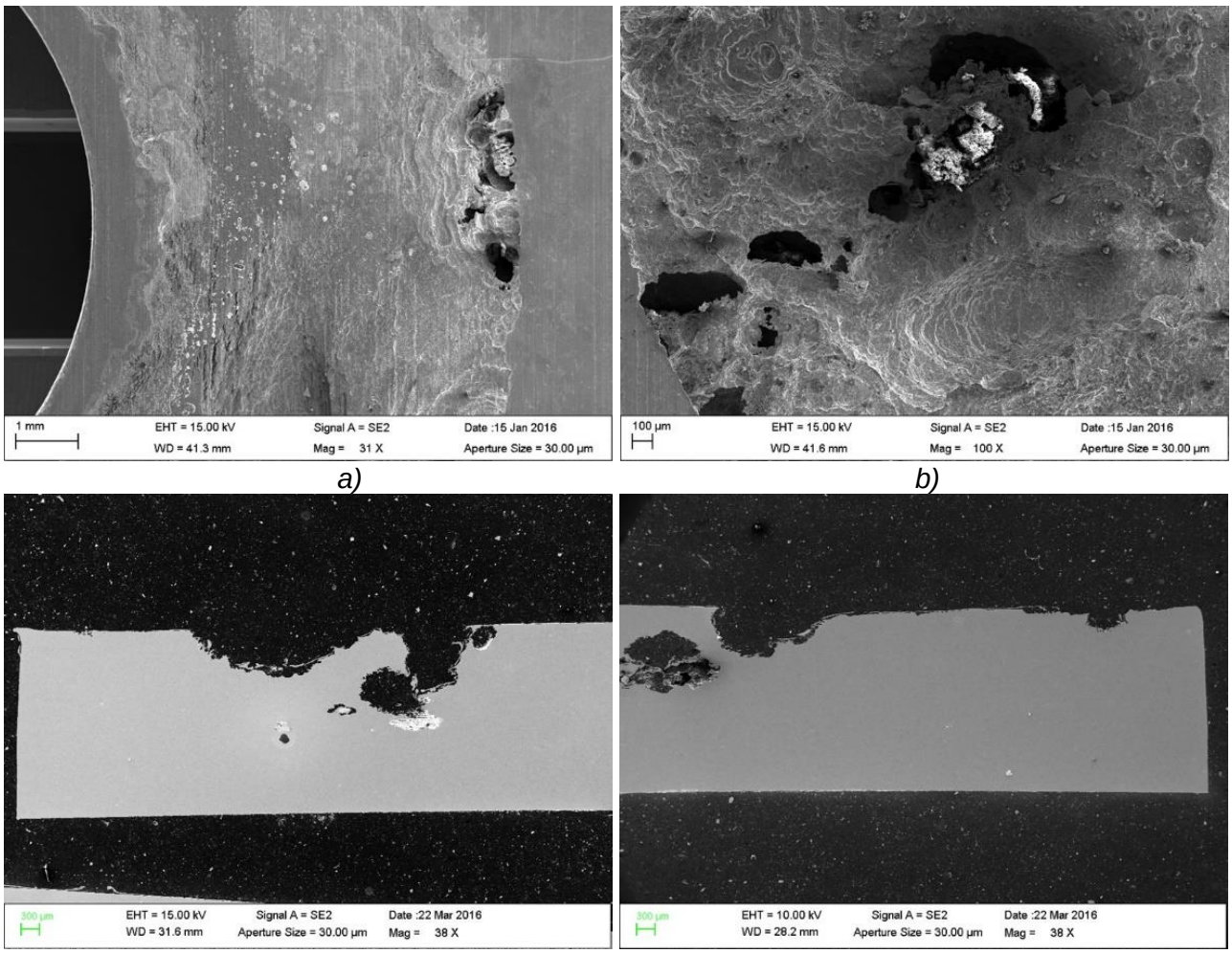

Figure 5. SEM images showing the corrosion attack in grade 904L in Solution 4 with 0.5 g/l Fe^{3+}. a, b) Top view. c, d) Cross-sectional view. Photographs are from experiments employing flat crevice formers.

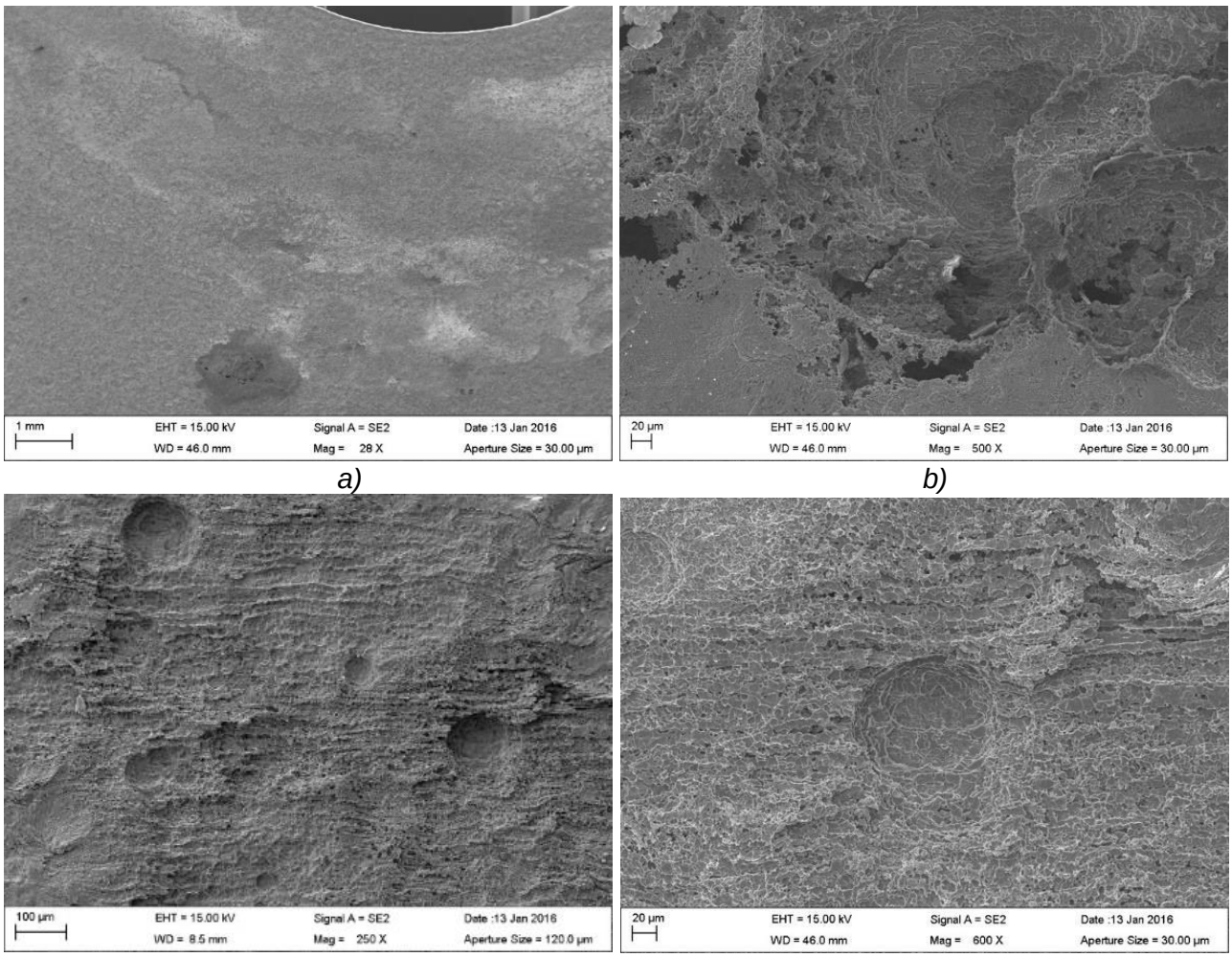

Figure 6. Top-view SEM images showing the corrosion attack in grade 2205 in Solution 4 with 0.5 g/l Fe^{3+}. Photographs are from experiments employing flat crevice formers.

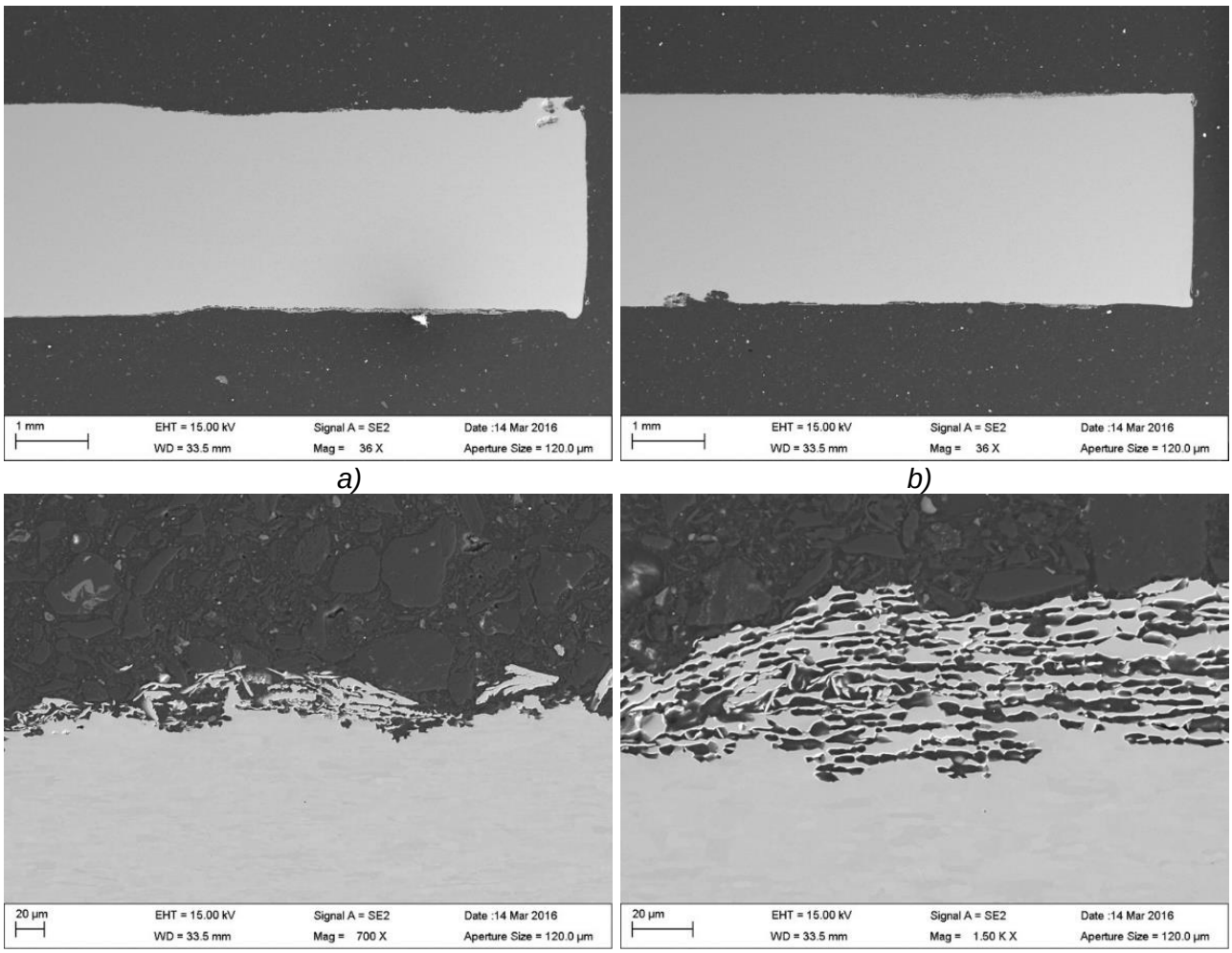

Figure 7. Cross-sectional SEM images showing the corrosion attack in grade 2205 in Solution 4 (0.5 g/l Fe^{3+}). Photographs are from experiments employing flat crevice formers.

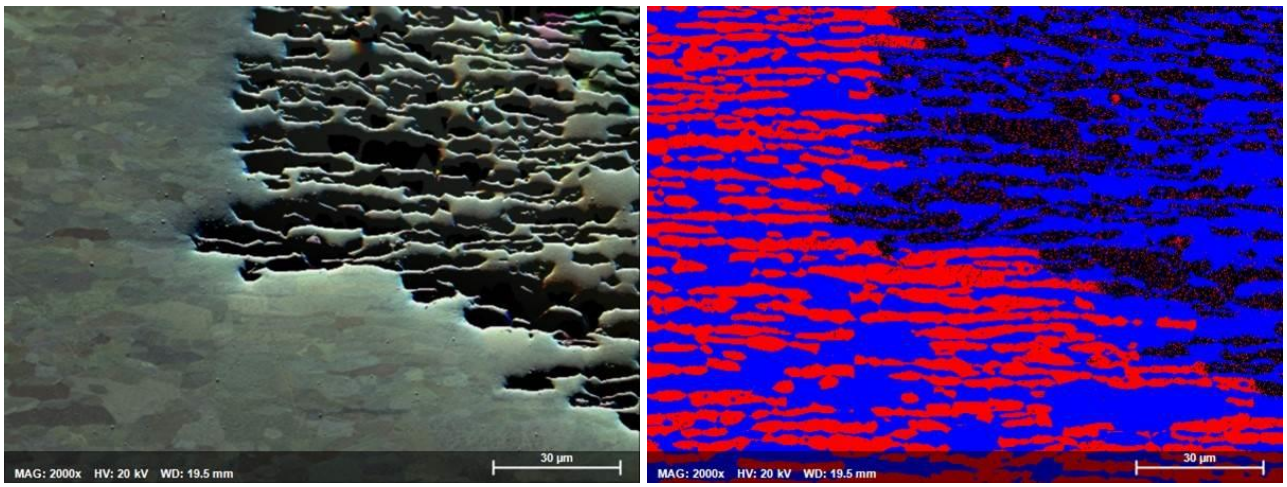

a) *b)*

Figure 8. Cross-sectional SEM image (a) and the corresponding EBSD band contrast map (b) for grade 2205 in Solution 4 (0.5 g/l Fe^{3+}). In b), the detected fcc phase, i.e., austenite, is shown in red and the bcc phase, i.e., ferrite, in blue. The images are from the tests carried out using serrated crevice formers, but the phenomenon and the extent of corrosion attack are similar in the specimens with flat crevice formers.

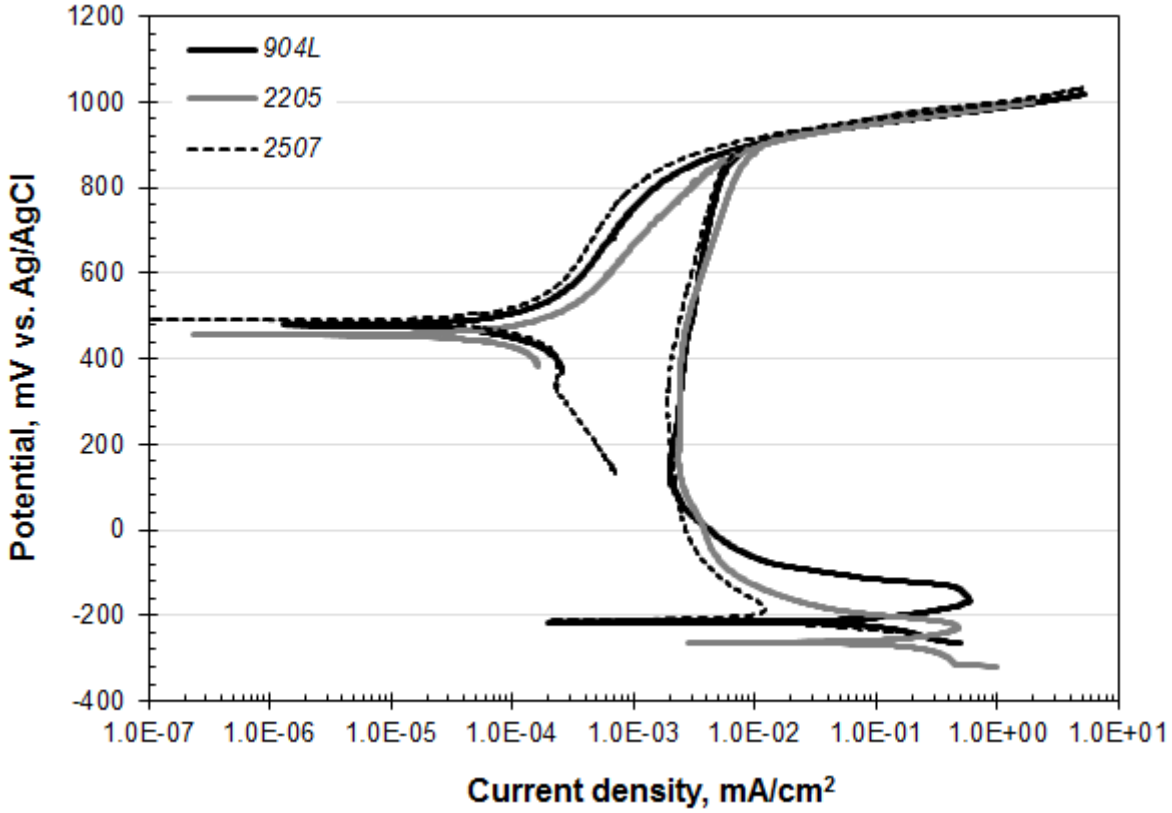

Figure 9. Polarization curves for the test materials. Solution: 50 g/l H_2SO_4, 1 g/l Cl^-, 90°C. Cl^- was added as HCl.

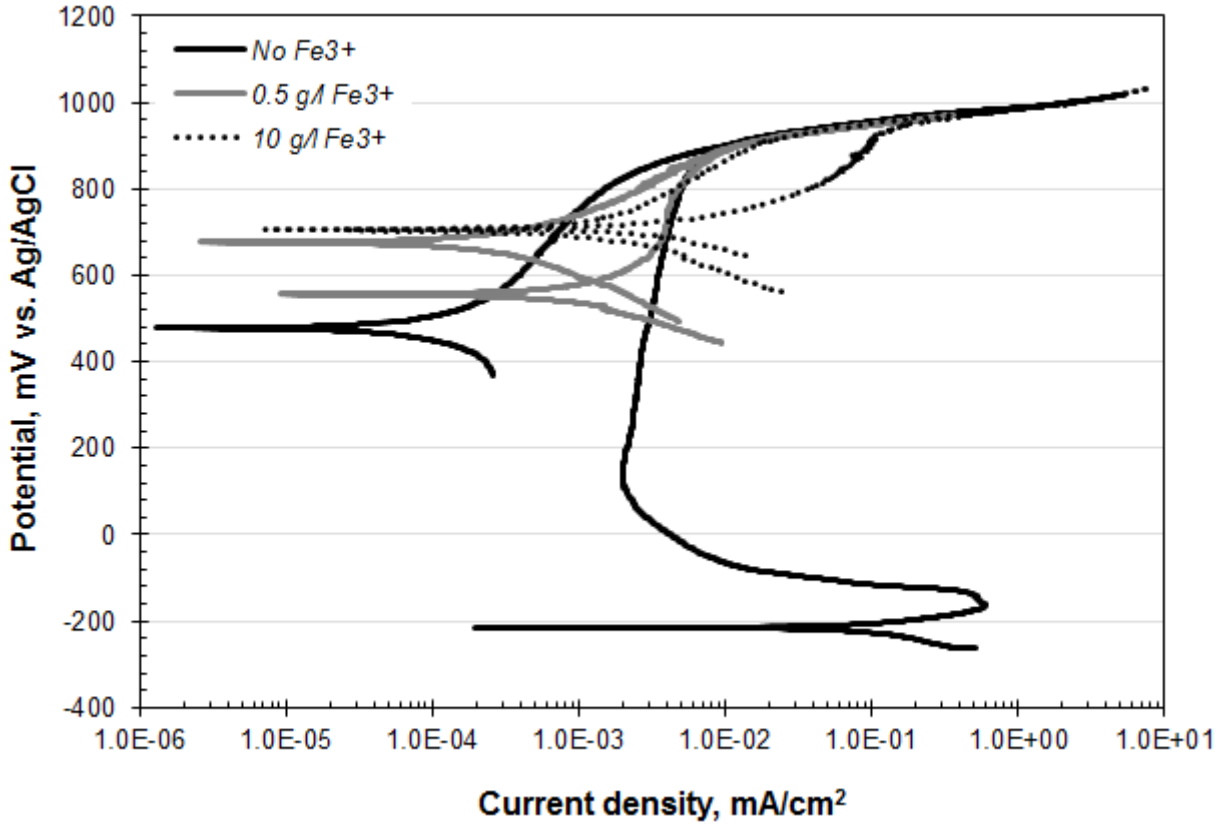

a)

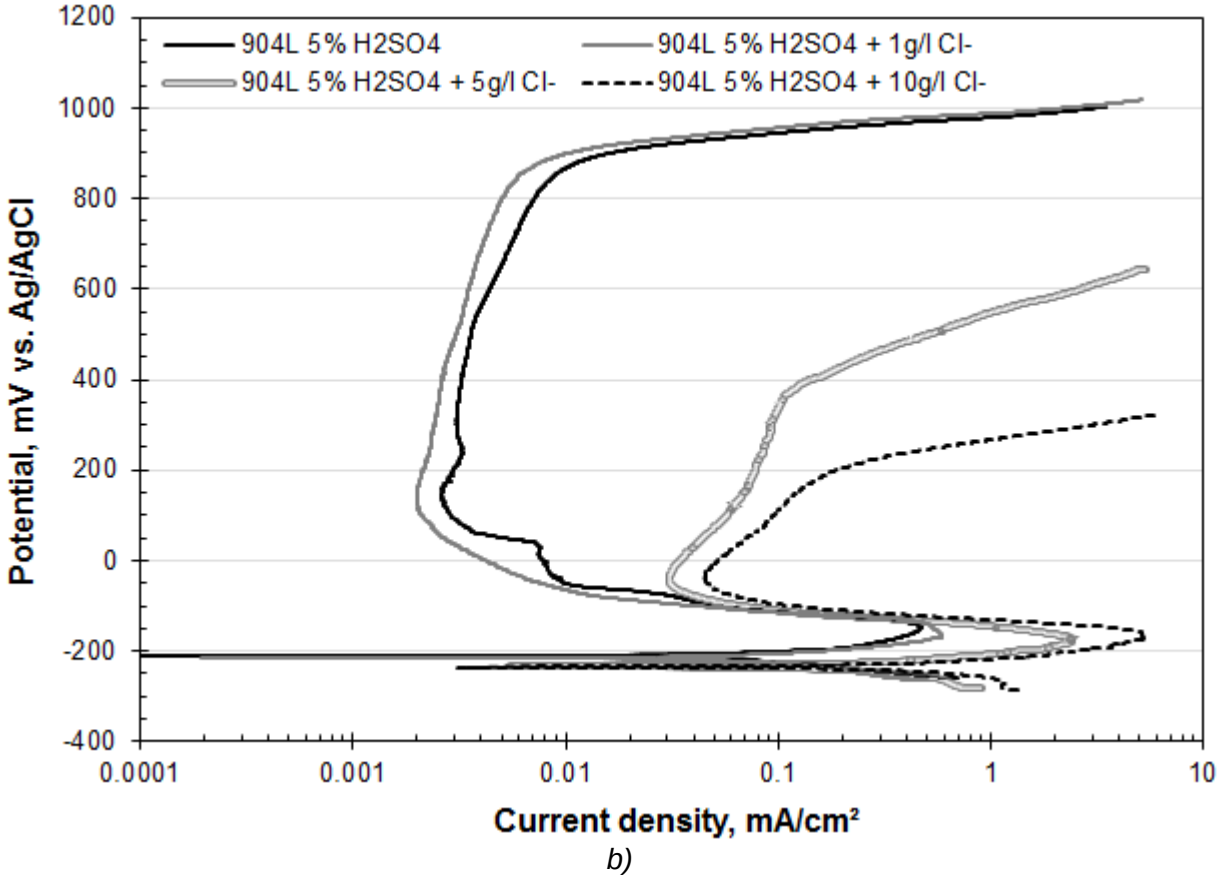

b)

Figure 10. Anodic polarization curves for 904L in the solution containing 50 g/l H_2SO_4, 90°C. a) Cl^- content 1 g/l. Without Fe^{3+}, with 0.5 g/l Fe^{3+}, and 10 g/l Fe^{3+}. b) As a function of Cl^- content. c) With and without SO_4^{2-} addition.

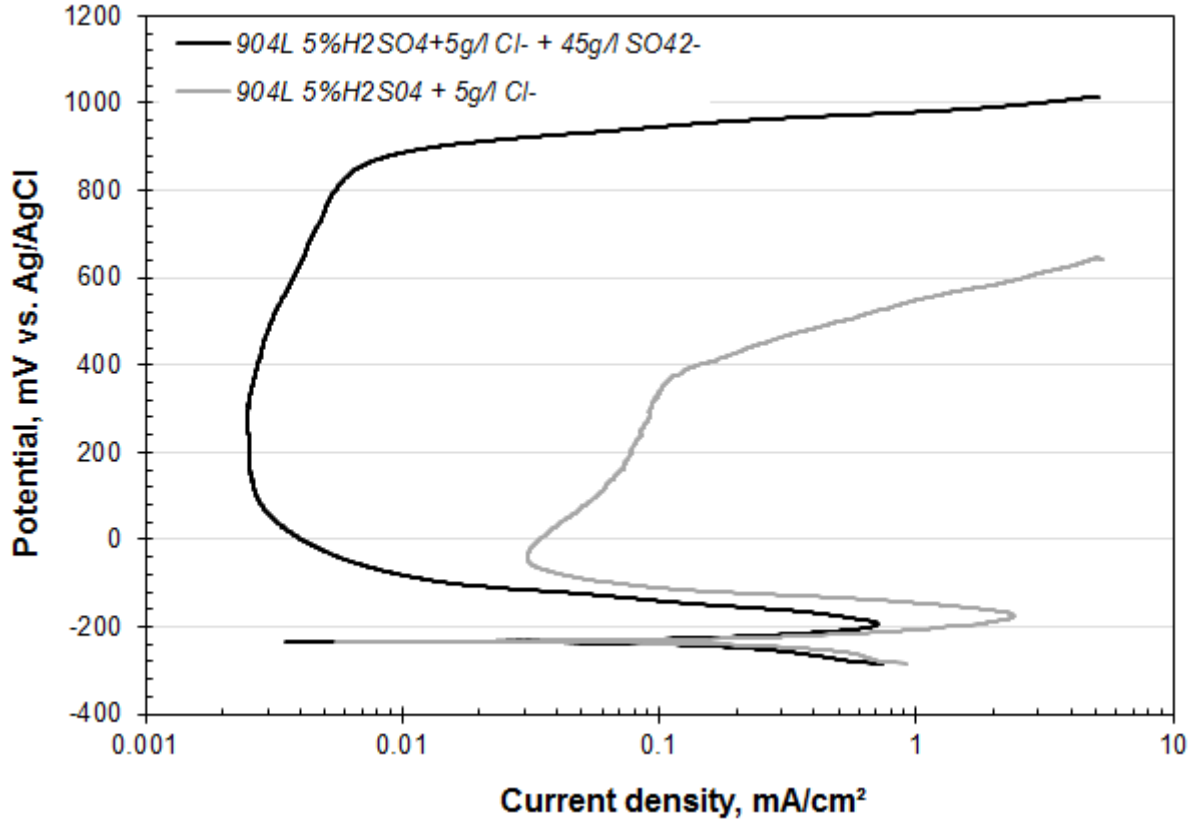

c)

Figure 10. Anodic polarization curves for 904L in the solution containing 50 g/l H_2SO_4, 90 °C. a) Cl^- content 1 g/l. Without Fe^{3+}, with 0.5 g/l Fe^{3+}, and 10 g/l Fe^{3+}. b) As a function of Cl^- content. c) With and without SO_4^{2-} addition.

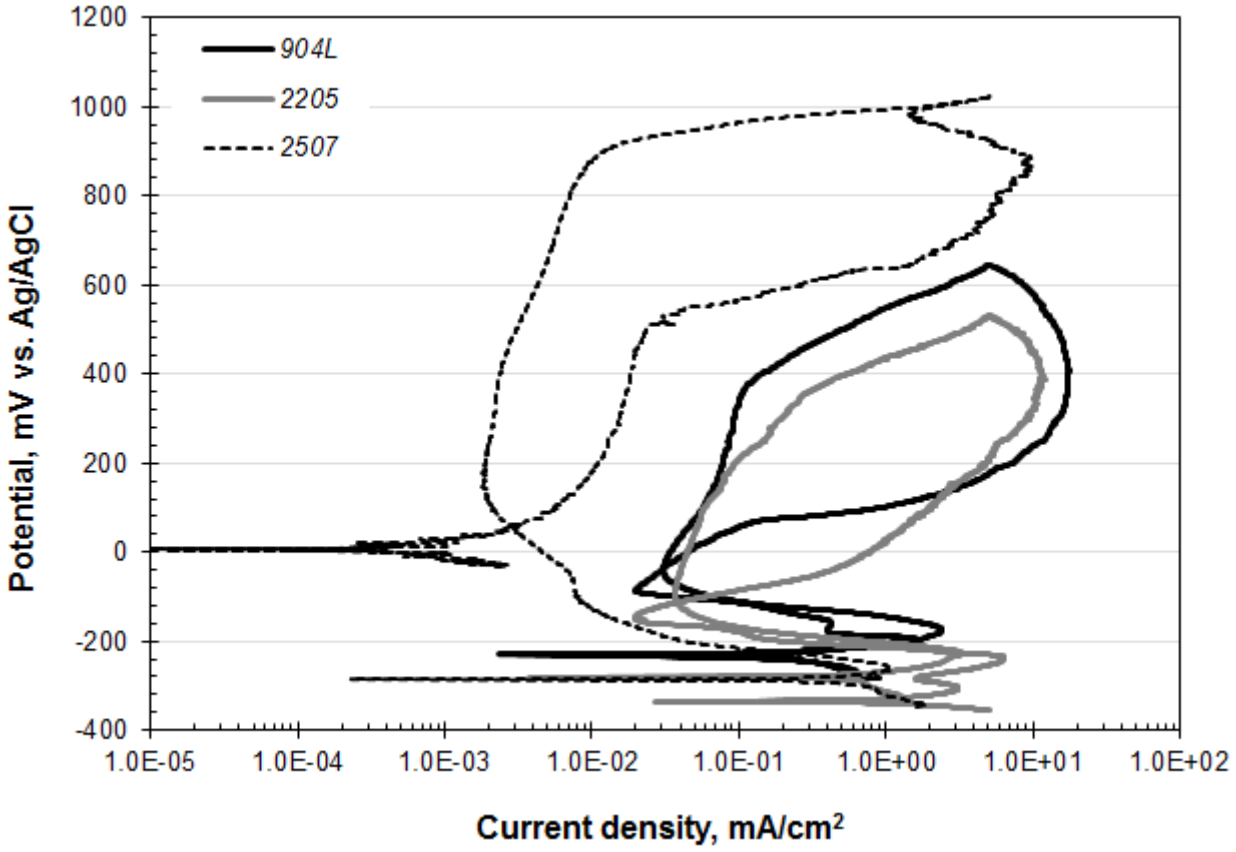

Figure 11. Cyclic anodic polarization curves for the three stainless steel grades in the solution containing 50 g/l H_2SO_4 and 5 g/l Cl^-, 90℃.

Table 1. Test materials, their nominal chemical compositions (in wt.%), and PREN-values.

Grade	EN	Microstructure	C	N	Cr	Ni	Mo	Others	PREN
904L	1.4539	Austenitic	0.01	-	20	25	4.3	1.5Cu	34
2205	1.4462	Duplex	0.02	0.17	22	5.7	3.1	-	35
2507	1.4410	Duplex	0.02	0.27	25	7	4	-	43

Table 2. Target compositions of the solutions.

Solution	H_2SO_4, g/l	Cl^-, g/l	Fe^{3+}, g/l	Cu^{2+}, g/l	Fe^{2+}, g/l
1	50	1	5	-	-
2	50	1	-	5	-
3	50	1	-	-	5
4	50	1	0.5	-	-

Table 3. Analyzed values of the test solutions before the tests.

Solution	H_2SO_4, g/l	Cl^-, mg/l	Fe^{3+}, mg/l	Fe(tot), mg/l	Cu^{2+}, mg/l	Redox at 23°C, mV vs. Ag/AgCl	Redox at 90°C, mV vs. Ag/AgCl	pH at 23°C	pH at 90°C
1	52.7	942	5100	5110	<1	507	676	0.31	0.66
2	52.6	940	-	<1	5220	294	440	0.27	0.49
3	52.0	970	370	5250	-	338	443	0.35	0.44
4	52.1	1170	550	574	-	409	675	0.32	0.57

Table 4. Summary of the calculated activities and pH. Chloride to sulfate activity ratio was calculated two ways: using target concentrations and measured concentrations of the solutions.

Solution	$a(Cl^-)$	$a(SO_4^{2-})$	$a(Cl^-)/a(SO_4^{2-})$ calculated based on measured concentrations	$a(Cl^-)/a(SO_4^{2-})$ calculated based on target concentrations	Calculated pH, T=23°C	Calculated pH, T=90°C
1 (5 g/l Fe^{3+})	0.011	0.0016	7.2	7.6	0.37	0.50
2 (5 g/l Cu^{2+})	0.017	0.0017	9.8	10.4	0.32	0.43
3 (5 g/l Fe^{2+})	0.017	0.0019	9.2	9.8	0.35	0.47
4 (0.5 g/l Fe^{3+})	0.019	0.0012	15.5	13.9	0.31	0.39

Table 5. Analyzed values of the test solutions after the tests.

Solution	H_2SO_4, g/l	Cl^-, mg/l	Fe^{3+}, mg/l	Fe(tot), mg/l	Cu^{2+}, mg/l	pH at 90°C
1	59.7	1130	1306	8450	16	0.42
2	54.6	1010	-	66	5490	0.44
3	51.5	955	1320	5630	-	0.43
4	52.1	1150	270	985	-	0.41

Table 6. Summary of the observed forms of corrosion in the case of both crevice former types.

Flat crevice formers				
Solution	Oxidant	904L	2205	2507
1	5 g/l Fe^{3+}	Crevice corrosion	Crevice corrosion & Edge corrosion	No corrosion
2	5 g/l Cu^{2+}	Crevice corrosion	No corrosion	No corrosion
3	5 g/l Fe^{2+}	Edge pitting	No corrosion	No corrosion
4	0.5 g/l Fe^{3+}	Crevice corrosion	Crevice corrosion	No corrosion
Serrated crevice former				
Solution	Oxidant	904L	2205	2507
1	5 g/l Fe^{3+}	Crevice corrosion	Crevice corrosion	No corrosion
2	5 g/l Cu^{2+}	No corrosion	No corrosion	No corrosion
3	5 g/l Fe^{2+}	No corrosion	No corrosion	No corrosion
4	0.5 g/l Fe^{3+}	Crevice corrosion	Crevice corrosion	No corrosion

Table 7. Average composition of the phases present in stainless steel grades 2205 and 2507 determined by five EDS analyses, and calculated PREN-values.

Grade		Fe	Cr	Ni	Mo	Si	Mn	PREN
2205	Austenite	68.0	21.2	6.6	2.4	0.4	1.4	31
2205	Ferrite	66.1	24.0	4.3	4.0	0.5	1.2	37
2507	Austenite	63.6	24.1	8.2	3.1	0.3	0.8	38
2507	Ferrite	66.1	27.1	5.2	4.8	0.3	0.6	44

Table 8. Calculated values for the activities of chlorides and sulfates as well as their ratio in the solutions used for the electrochemical measurements.

Solution	H_2SO_4, g/l	Cl^-, g/l	SO_4^{2-}, g/l	Fe^{3+}, g/l	a(Cl^-)	a(SO_4^{2-})	a(Cl^-) /a(SO_4^{2-})
Base solution	50	1			0.018	0.0012	15.1
Addition of ferric iron	50	1		0.5	0.0066	0.0013	5.3
	50	1		10	0.0000025	0.0021	0.0012
Influence of Cl^- content	50	0				0.0013	0
	50	5			0.090	0.0010	87.9
	50	10			0.18	0.00087	206.5
Addition of sulfate	50	5	45		0.087	0.0044	19.8